Desalination and Water Treatment
www.deswater.com

doi:10.5004/dwt.2019.24393

164 (2019) 192–205
October

Preparation of functionalized CuO nanoparticles using *Brassica rapa* leave extract for water purification

Bushra Fatima, SharfIlahi Siddiqui, Rabia Ahmed*, Saif Ali Chaudhry*

Department of Chemistry, Jamia Millia Islam, New Delhi-110025, India, email: rahmad@jmi.ac.in (R. Ahmed), saifchaudhry09@gmail.com (S.A. Chaudhry)

Received 15 August 2018; Accepted 13 May 2019

ABSTRACT

The functionalized-CuO nanoparticles were synthesized by following an eco-friendly, green route using Brassica leaf extract. The prepared monoclinic crystals of functionalized-CuO nanoparticles have size around 50 nm with point of zero charge at pH 7.7. The EDX investigation indicated that the functionalized-CuO NPs possessed C (18.50%), Cu (28.33%), and O (53.16%) elements by weight, the presence of content clearly indicated the formation and functionalization of CuO NPs. The prepared nanoparticles of smaller size have high surface area, the primary criteria for a good adsorbent, were used as an adsorbent for Amaranth, Congo red, and Bismarck brown dyes, however, the detailed studies were carried out for Amaranth dye only. The batch adsorption experiments were performed to optimize the pH, Amaranth dye concentration, reaction time, dose of functionalized-CuO NPs, and temperature, to get maximum adsorption and then performed actual experiments. The study has shown that more than 90% adsorption of Amaranth dye from its solution, having 10 mg L^{-1} concentration, was achieved with 2.0 g L^{-1} of dosage of functionalized-CuO NPs. For determining the adsorption capacity of these nanoparticles for Amaranth dye, and to propose mechanism of the adsorption process the data adsorption was fitted into non-linearized Langmuir, Freundlich, and Dubinin-Radushkevich isotherms. The Langmuir capacity of CuO NPs decreased from 55.33 to 33.17 mg g^{-1} when the temperature of the reaction mixture was raised from 27 to 45°C. The thermodynamic study showed that the process was feasible and endothermic in nature. The reaction kinetics revealed that the Amaranth dye adsorption followed pseudo-second order.

Keywords: Biogenic; CuO; Wastewater; Dye; Amaranth; Adsorption

1. Introduction

Wastewater "A mixture of harmful metal ions, dyes, bacteria, pathogens, fungi, solvents, and other toxic chemicals" is found to be the major cause of water pollution which adversely affects the ecosystem. Dyes are colour producing organic compounds which are used in textile industries, that consume huge amount of water in dyeing process, and release effluents that is a major player for water pollution [1,2]. Dyeing materials, particularly azo dyes, are non-biodegradable, and highly poisonous organic compounds [3–6].Among various dyes, Amaranth {Trisodium (4E)-3-oxo-4-[(4-sulphanato-1-naphthyl)hydrazono]naphthalene-2,7-disulphonate}, AM, an anionic azo dye, synthesized from petroleum products, is employed to colour both natural and synthetic fibers, paper, leather, and other resins, and thus found in industrial wastewater. When ingested, through contaminated water, it causes many harmful effects, including allergy, respiratory problems, and birth defects, and generation of cancerous tumours [7–9].

For providing safe drinking water, these pollutants should be removed, for which various approaches like ion-exchange, flocculation, electrolysis, coagulation, biodegradation, photocatalytic degradation, chemical oxidation, precipitation, and adsorption, have been adopted. But, among them the adsorption i.e., adhesion of dye molecules

*Corresponding author.

from water onto the solid surface is the most promising one because of the simplicity, inexpensiveness, sludge free, high efficiency, and good biocompatibility [10–14]. Nanomaterials, as adsorbent, can be employed effectively for the treatment of wastewater to remove the harmful dyes to make water suitable for human consumption. Various kinds of nanomaterials have been prepared and utilized for water treatment [15]. But the preparation of nanomaterials through conventional chemical routes involves application of various toxic chemicals which produce toxic waste. However, the synthesis of nanomaterials though green-route can overcome the generation of toxic waste which can take top position in nanotechnology over the physical and chemical routes.

The environmentally benign, inexpensive synthesis of nanoparticles without using traditional chemicals and toxic solvent could be achieved by involving plant extract (leaves, flower, fruits, roots,and stems). In the past various metal oxide nanoparticles have been utilized for water treatment [16–19]. In literature, copper oxide, CuO, an amphoteric oxide, have been prepared in conventional method and investigated for a wide range of applications including catalytic activity, antimicrobial activity, semiconductors, sensors and for water treatment to remove dyes and other pollutants [20]. However, the density of active sites on the surface of CuO NPs, for attracting pollutants, is usually low which can be enhanced to attract more pollutants by enhancing the presence of functional groups on their surface. Therefore, for the better water treatment efficiency of CuO NPs can be enhanced by its surface functionalization. But the functionalization of adsorbing materials is usually carried out through traditional methods which create ultimately water pollution [21].

The functionalization can be carried using plant extract that contains abundant phytochemicals and can also act as reducing, capping, and stabilizing agents for NPs. In the past CuO NPs have been synthesized by employing various plant extracts including *Gloriosa superba* leave, *Aloe vera* leave, *Ixora coccinea* leave, *Olea europaea* leave,tea leave, coffee powder, and *Daphnia magna* [22–27]. The objective of the present work, synthesis of functionalized copper oxide nanoparticles, functionalized-CuO NPs, was achieved by following a green pathway using *Brassica rapa* leave extract. *Brassica rapa* leave extract contains non-toxic health-promoting phenolic flavonoids including *quercetin*, *kaempferol*, *isorhamnetin*, *anthocyanins*, and non-flavonoids such as derivatives of cinnamic acid which along with synthesis may functionalize the CuO NPs [28].

The prepared functionalized-CuO NPs were employed as an adsorbent for the elimination of toxic Amaranth, AM dye from aqueous solution. The adsorption process was studied in terms of contact time, dosage of functionalized-CuO NPs, pH of solution, solution temperature, and dye concentration. For explaining the mechanism, involved during the adsorption, the data was fitted in different isotherm, kinetic, and thermodynamic parameters yielding relationships. The isotherm, kinetic, and thermodynamic variables were utilized to determine the adsorption capacity, reaction speed, feasibility, and spontaneity of the process. Furthermore, the adsorption capacity of the functionalized-CuO NPs, for AM dye, was also compared with adsorption capacity for Congo red and Bismarck brown R dyes.

2. Experimental section

2.1. Materials and methods

The *Brassicarapa* leaves were collected from the local garden of Jamia Millia Islamia, New Delhi, India, during winter season. Urea and precursor copper acetate dihydrate, $Cu(CH_3COO)_2{\cdot}2H_2O$, used for the fabrication of functionalized-CuO NPs were purchased from Merck Ltd., Germany. HCl and NaOH required for changing of pH of reaction system were procured from Merck Ltd., Germany. Amaranth (M_w = 604.473 g mol^{-1}, λ_{max} = 520 nm), Congo red (M_w = 696.665 g mol^{-1}, λ_{max} = 497 nm), and Bismarck Brown R (M_w = 461.39 g mol^{-1}, λ_{max} = 468 nm) dyes, for the preparation of solution, were procured from the Merck India. All the chemicals used in this study were used as such without any purification.

2.2. Preparation of plant extract

To prepare aqueous extract, the leaves of *Brassica rapa* were washed several times with distilled water for removing dust and other adherents from the surface. The healthy and undamaged leaves were grinded into thick paste with the help of mixer and grinder. 10 g leaves were added to 100 mL double distilled water and then heated to 50°C for 2 h and afterward filtered using Whatman filter paper.

2.3. Synthesis of functionalized CuO-NPs

The previously reported method was adopted for the green synthesis of functionalized-CuO NPs using *Brassica rapa* leave extract [29]. In brief, 25 mL aqueous extract was mixed with 20 mL of 0.2 mol L^{-1} copper(II) solution, and to this 0.1 mol L^{-1} urea solution was added, followed by addition of 10 mL of 1.0 mol L^{-1} NaOH solution. The mixture was kept in an oven at 50°C for 45 min and after that a blue colour precipitate was obtained that indicated the formation of CuONPs which has been shown schematically in Fig. 1. The coloured solution of CuO NPs was centrifuged at 1500 rpm for 10 min, washed with distilled water, and dried at 60°C for 24 h. Further, the resultant biogenic CuO NPs were characterized and used for the adsorption studies.

2.4. Characterization of functionalized-CuO NPs

The synthesized NPs were characterized with several spectroscopic and microscopic techniques including UV-Vis spectroscopy, Fourier transform infrared spectroscopy (FT-IR), powder X-ray diffraction (XRD), scanning electron microscopy (SEM) and with energy-dispersive X-ray spectroscopy (EDAX), and Tunnelling electron microscopy (TEM). The optical behaviour of the F-CuO NPs was characterized using UV absorption spectra. The functionalization of NPs was studied by FT-IR spectrum, in 4000–400 cm^1 range, recorded on VERTEX 70/70v (BRUKER) spectrometer in KBr. The structural properties of functionalized-CuO NPs were investigated by XRD analysis recorded on a Philips PW-3710 diffractometer (having Cu-Kα radiation, λ = 1.54 Å, a Cu-filter, operated at 35 kV generator voltage, 30 mA current, and fitted with proportional counter detector). The morphology of the prepared NPs was inves-

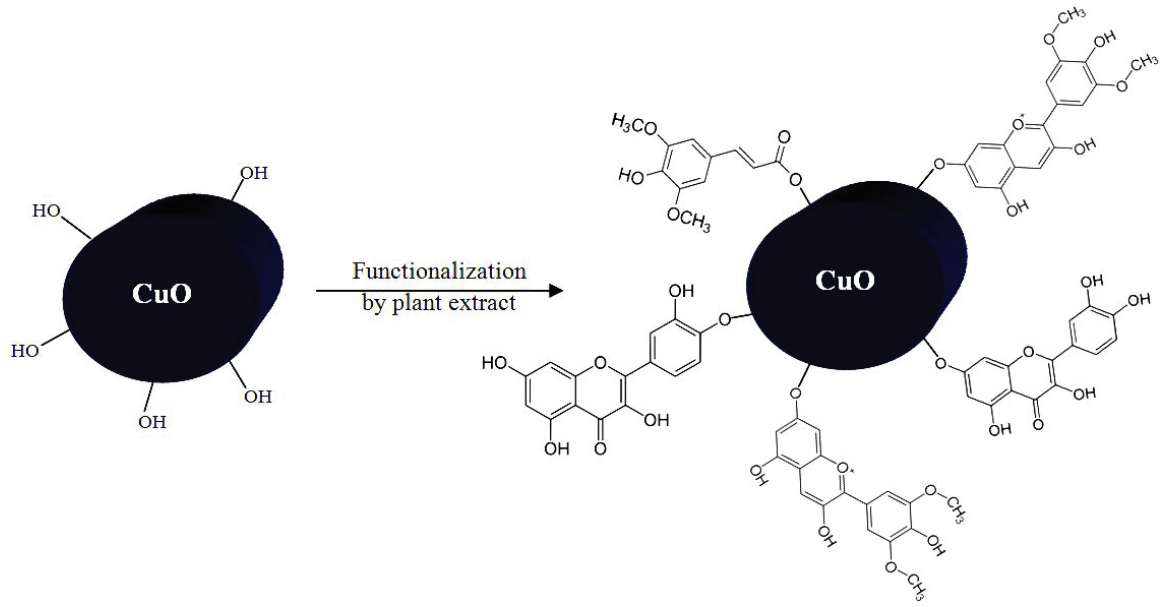

Fig. 1. Proposed scheme of functionalization of CuO NPs by organic compounds present in *Brassica rapa* leave extract.

tigated on the scanning electron microscope (FESEM Nova Nano SEM 450, FE1) equipped with EDAX (Bruker 127 eV). EDAX spectrum was recorded to investigate the elemental composition. The size and microstructure of the functionalized-CuO NPs were analyzed using high resolution TEM [Tecnai T-30 (300 kV FEGTEM)] operated at 80 kV.

2.5. Determination of pH_{zpc} (point of zero charge)

Point of zero charge (pH_{ZPC}) is pH of solution at which the submerged solid exhibits zero net electrical charge on the surface. In order to find out pH_{ZPC} of the F-CuO NPs, salt addition method was adopted by using 0.1 M NaOH and 0.1 M HCl solutions [30]. In brief, 0.01 mol L^{-1} KNO_3 aqueous medium was placed in six different flasks and the pH of the solutions was adjusted in 2–10 range by using NaOH and HCl solution and measured by pH meter (APX 175 E/C, Control Dynamics Instrumentation Pvt. Ltd., Bangalore, India). In each of them 20 mg functionalized-CuO NPs were added and then the flasks were agitated at 150 rpm for 120 min in water bath shaker at room temperature. After that the pH of each solution was measured and the final pH values were used to calculate the ΔpH (pH_i–pH_f) and a graph between ΔpH and pHi was plotted. The point of intersection of the two graphs represents the pH_{ZPC} of functionalized-CuO NPs [Fig. S1; Supplementary Information].

2.6. Adsorption studies

The batch mode adsorption experiments were performed to estimate the adsorption capacity of functionalized-CuO NPs for AM dye under the influence of adsorbent dosage, initial AM dye concentration, pH of the reaction mixture, contact time, and reaction temperature by mechanically agitating a series of 50 mL Erlenmeyer flasks containing mixture of 10 mL of AM dye solution of certain concentration, 5–30 mg of functionalized-CuO NPs at certain pH (2–10) and temperature. Isotherm parameters were determined by varying the concentration of AM dye from 10 to 60 mg L^{-1} at 27, 35, and 45°C. Contact time effect was investigated with 20 mg L^{-1} concentration of AM dye, 2.0 g L^{-1} functionalized-CuO NPs at room temperature to determine the kinetic parameters of the reaction as well as the optimum time required for maximum dye removal. After each set of adsorption experiments, the dye solutions were centrifuged to separate the sorbent from the solution and the remaining concentration of AM dye was analyzed using ultraviolet-visible (UV-Vis) spectrophotometer (T80-UV/VIS, PG Instruments Ltd., Leicestershire, England) at 528 nm. The removal percentage of AM dye as calculated using the relationship [31].

$$\%\ adsorption = \left(\frac{C_o - C_e}{C_o}\right)100 \tag{1}$$

where C_o and C_e are initial and final concentrations of AM dye in the solution (calculated from calibration curve) [Fig. S2; Supplementary Information]. The equilibrium uptake capacity of functionalized-CuO NPs was estimated using the relationship:

$$Q_e = (C_o - C_e)\frac{V}{m} \tag{2}$$

where Q_e (mg g^{-1}) is the amount of AM dye adsorbed onto the unit mass of functionalized-CuO NPs at equilibrium, m (g L^{-1}) is mass of functionalized-CuO NPs and V (mL) the volume of AM dye solution.

2.7. Regeneration and reusability of exhausted adsorbents

Regeneration and reusability of a used adsorbent is an important step to achieve a reliable and inexpensive water treatment technique. The regeneration involves separation of an adsorbent from reaction solution followed by the

detachment of loaded adsorbate from the surface though tuning the solutions pH. For this study, alkaline solution was used to desorb the AM dyes from loaded functionalized-CuO NPs. Briefly, AM dye loaded functionalized-CuO NPs was added to 50 mL Erlenmeyer flask containing 0.1 M NaOH solution, shacked for 6 h in water bath incubator shaker at room temperature and 200 RPM, and then the regenerated functionalized-CuO NPs was washed with distilled water and dried, and then reutilized for three adsorption-desorption cycles.

3. Result and discussion

3.1. Characterization of functionalized-CuO NPs

The FT-IR spectrum of biologically synthesized functionalized-CuO NPs, shown in Fig. 1, ascribed the presence of –OH and C-O groups on the surface. The broad absorption band in the range 3050–3650 cm^{-1} was assigned to the -O-H stretching vibrational frequency. The bands around 960 and 1456 cm^{-1} reflected the C-O stretching vibrations and that at 1610 cm^{-1} were assigned to the C=O stretching and N-H bending of amide group. The bands in the range 750–450 cm^{-1} were assigned for the vibrational modes of functionalized-CuO NPs. The major M-O bands appeared at 480, 597, and 695 cm^{-1} indicated the formation of the monoclinic phase of CuO NPs [32]. This FT-IR spectrum of biologically synthesized CuO NPs using organic compounds present in the *Brassica rapa* leave extract also suggested the functionalization of CuO NPs (Fig. 3). The FT-IR spectrum of dye loaded-CuO NPs was used to indicate characteristics absorption band of AM dye present on CuO NPs. The spectrum indicated all the similar bands to those of unloaded functionalized-CuO NPs as well as new bands at 1497, 1195, and 1039 cm^{-1}. The vibration band at 1497 cm^{-1} was assigned for the azo groups (-N=N-) of AM dye, and the peaks around 1195 and 1039 cm^{-1} for the anti-symmetric stretching frequency of $-SO_3^-$ group of AM dye, and that due to coupling between benzene ring and the SO_3 group. These peaks assigned in loaded adsorbent gave the evidence for adsorption of AM dye onto the functionalized-CuO NPs as shown in Fig. 3 [33]. The shifting of characteristics bands, corresponding to -OH and C-O groups, towards the lower wavenumbers were also observed in Fig. 3. The shifting of the characteristic bands of functionalized-CuO NPs suggested the hydrogen bonding and electrostatic interaction between the functionalized-CuO NPs and dye molecules (Fig. 2).

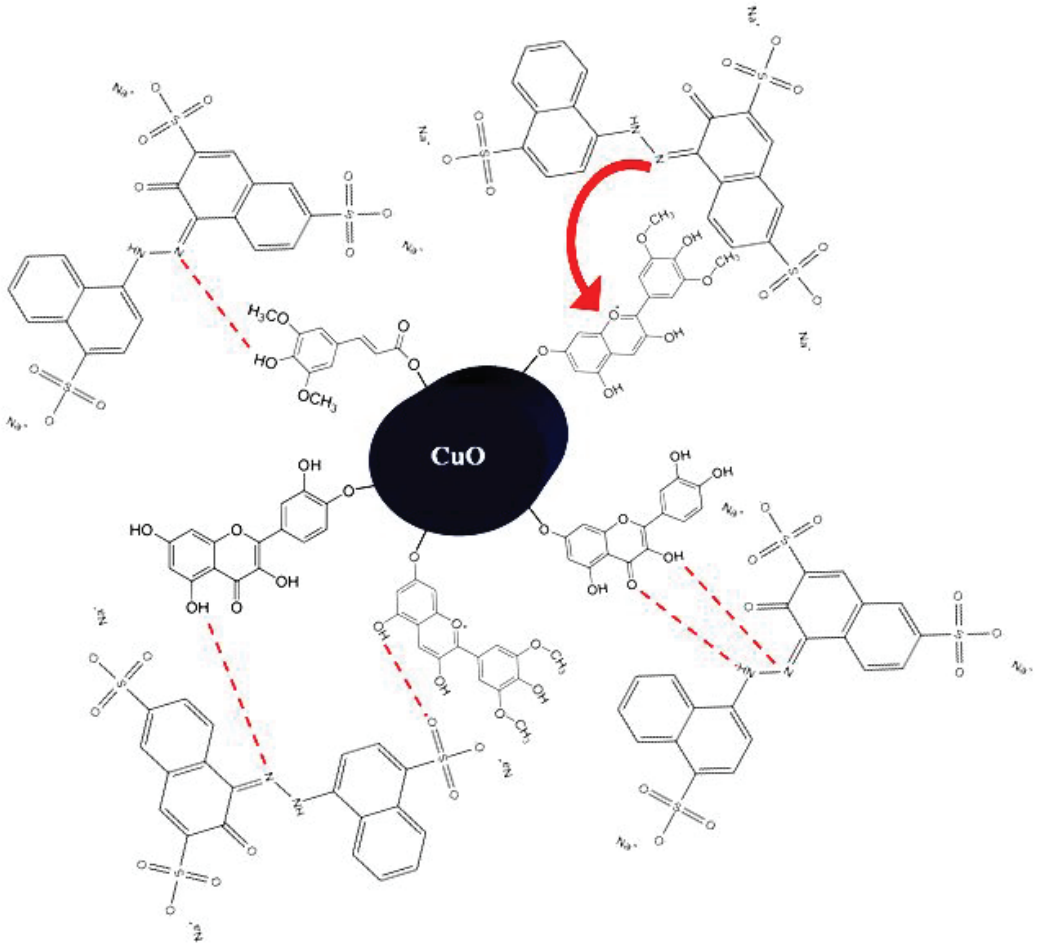

Fig. 2. Possible adsorptive interaction between the AM molecules and functionalized-CuO NPs.

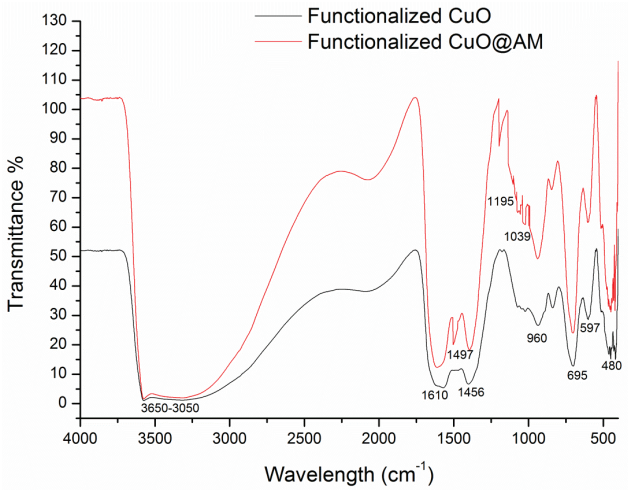

Fig. 3. FT-IR spectrum of functionalized-CuO NPs (black) and Amaranth dye loaded functionalized-CuO NPs (red).

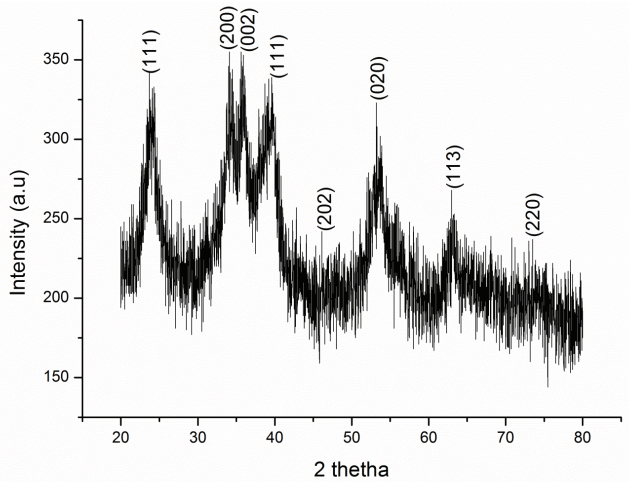

Fig. 4. XRD pattern of functionalized-CuO NPs.

Powder XRD technique was employed to characterize biogenic CuO NPs by scanning in the angular range 10–80° (2θ) with a step size of 8.0° min^{-1}. The XRD pattern of CuO NPs (Fig. 4) shows the peaks at 36°, 38°, 48°, 56°, and 64° (2θ) corresponding to the [002], [111], [202], [020] and [113] planes, respectively, of CuO NPs. All these reflection peaks of CuO NPs can be indexed to the monoclinic crystal system of CuO NPs (JCPDS card no. 45-0937) [34,35]. The weak diffraction peaks indicated somehow amorphous nature of the prepared NPs. There were some impurities which appeared in the diffraction peaks due to Cu metallic NPs which appeared at 26.4° [111], 34.1° [200], 70.10° [220] [35]. The crystallite size of the functionalized-CuO NPs was estimated by using highest intensity XRD peak data in the Scherer's equation [36]:

$$D = \frac{K\lambda}{\beta \mathrm{Cos}\theta} \tag{3}$$

where K = 0.9, and λ = 1.54A are shape factor, and X-ray wavelength of Cu-Kα radiation, respectively. Also α and β are Bragg diffraction angle, and FWHM of the respective diffraction peak. The crystallite size corresponding to the highest peak observed in XRD was found to be 15 nm. The presence of weak structural peaks in XRD pattern, and crystallite size, suggested the amorphous nature of functionalized-CuO NPs.

The morphology of the prepared functionalized-CuO NPs was investigated from SEM imaging (Fig. 5) which indicated irregular particles of various sizes. The functionalized-CuO NPs appeared in as flower shapes. The aggregation of some particles occurred due to high surface energy and negative enthalpy due to van der Waal forces of attraction between particles.

The EDX analysis indicated the chemical composition of CuO NPs that possessed C (18.50%), Cu (28.33%), and O (53.16%) elements by weight (Fig. 6). The average diameter of the functionalized-CuO NPs range was observed in the 50 nm range from TEM studies (Fig. 7).

UV-Visible spectroscopic technique was employed for the detection of surface plasmon resonance, SPR, which is

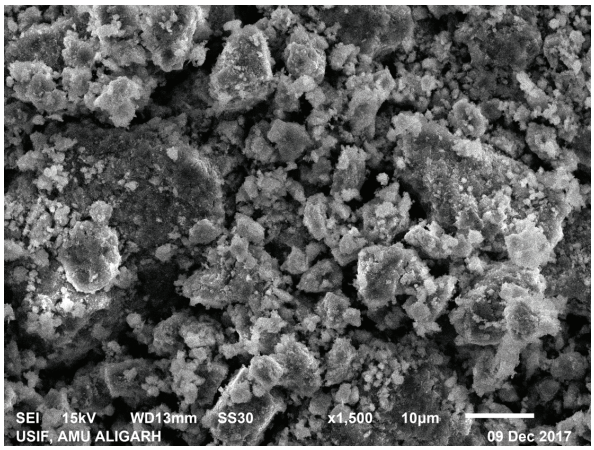

Fig. 5. SEM image of functionalized-CuO NPs.

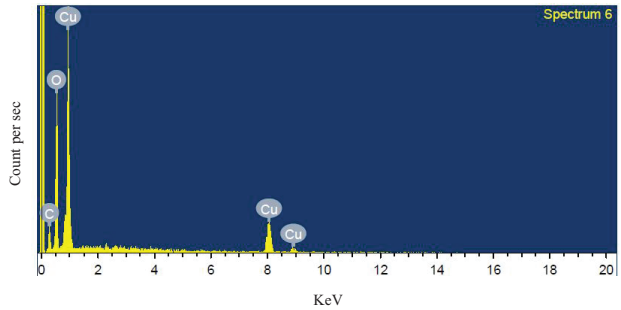

Fig. 6. SEM-EDX graph for elemental analysis of functionalized-CuO NPs.

the characteristic of NPs. The SPR band was observed at 231 nm (Fig. 8) which indicated the preparation of CuO NPs. The characteristic peak for CuO NPs usually occurs at 240 nm but in this case shifted to 231 nm or towards higher energy which can be correlated to the reduction in particles size of functionalized-CuO NPs formation that could also be confirmed from the peak tail. Moreover, in the UV-visible spectra only

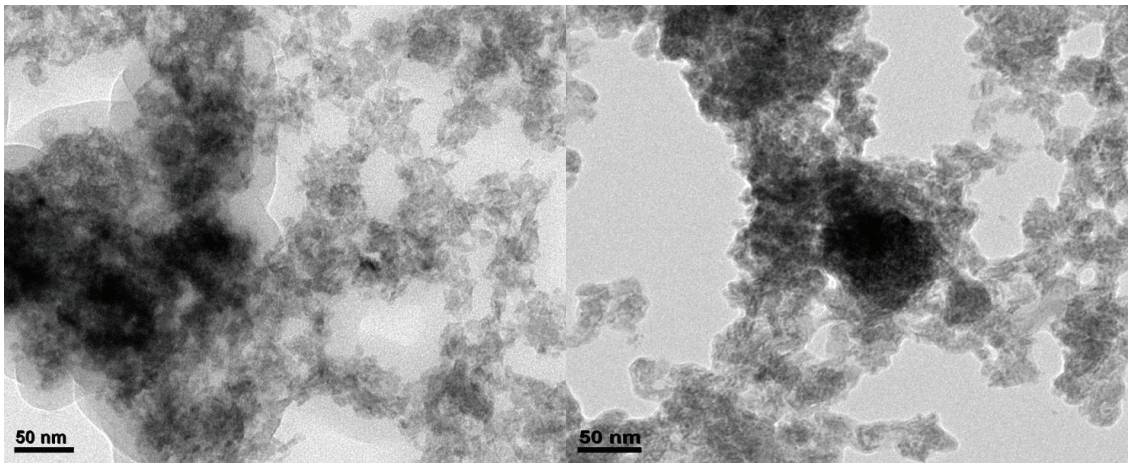

Fig. 7. TEM image of functionalized-CuO NPs at different magnifications.

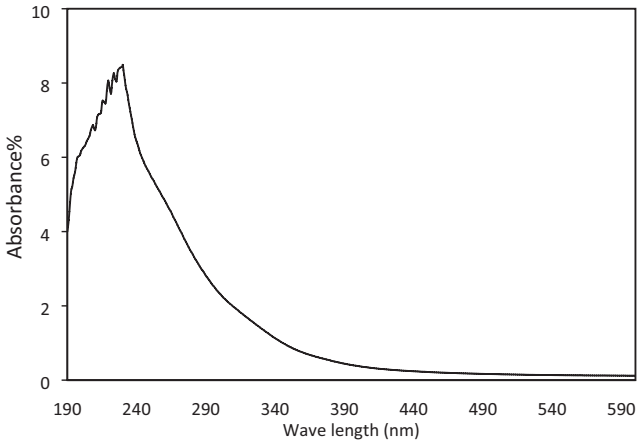

Fig. 8. UV-Visible absorption spectrum of functionalized-CuO NPs.

a single plasmonic peak was observed which indicated the formation of nearly spherical shaped CuO NPs [37].

3.2. Zeropoint charge of functionalized-CuO NPs surface

The zero point charge of the functionalized-CuO NPs surface was investigated [Fig. S1; Supplementary Information] and found at pH 7.7, means the pH point at which the CuO do not acquire any charge on the surface. The pH of the solution above and below pH 7.7 creates negative and positive charge at the surface of CuO NPs, respectively. These variations in the charges may govern the trends of adsorption of AM dye onto the functionalized-CuO NPs surface at various pHs.

3.3. Adsorption studies

3.3.1. Effect of functionalized-CuO NPs dosage

In order to investigate the influence of amount of functionalized-CuO NPs on the adsorption of AM dye, five 50 mL Erlenmeyer flasks having 10 mL dye solution (of 20 mg L^{-1} concentration) and 1, 1.5, 2.0, 2.5 and 3.0 g L^{-1}amount of functionalized-CuO NPs were agitated at 150 rpm. The experiment showed that with the increase of amount of functionalized-CuO NPs from 1.0 to 1.5 g L^{-1} the percentage of dye adsorbed increased from 35 to 72% which further increased up to 99% on increasing the amount to 3.0 g L^{-1} (Fig. 9a). This adsorption trend was due to the reason that with the increase in adsorbent dosage the number of adsorption sites also increased proportionally, thus adsorption capacity increased with the increase in amount of functionalized-CuO NPs. 2.0 g L^{-1} dosage of functionalized-CuO NPs was sufficient for 20 mg L^{-1} concentration of AM dye with which more than 92% of AM dye got removed from aqueous media,therefore, for further studies 2.0 g L^{-1} dose of CuO was used.

3.3.2. Effect of dye concentration

The effect of concentration on the adsorption phenomena is investigated by varying the concentration of dye and then studying the adsorption capacity. The effect of AM dye concentration on the adsorption onto functionalized-CuO NPs was investigated by varying the concentration from 10 to 60 mg L^{-1} at 30ºC with fixed dosage of 2.0 g L^{-1} of CuO NPs. The removal efficiency of functionalized-CuO NPs decreased from 92 to 87% when the concentration of AM dye was increased from 10 to 60 mg L^{-1} (Fig. 9b). This may be due to availability of limited surface area at optimum dosage and higher concentration gradient mass remained unadsorbed in aqueous phase. Moreover, results obtained revealed that 2.0 g L^{-1} functionalized-CuO was sufficient for the removal of AM dye from 10 to 60 mg L^{-1} concentration. At 20 mg L^{-1} of initial concentration of AM dye, more than 90% of AM dye could be removed from aqueous solution, therefore, 20 mg L^{-1} of initial concentration of AM dye was chooses as optimum concentration for further studies.

3.3.3. Effect of solution pH

The pH of water also affects the adsorption capacity of a material for a particular adsorbate by changing the charge on the adsorbent surface and/or adsorbate speciation. At alka-

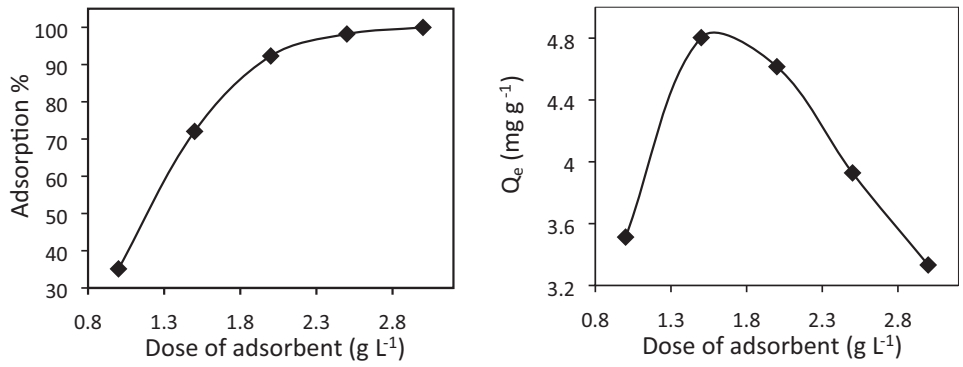

Fig. 9a. Effect of amount of functionalized-CuO NPs onto AM removal efficiency.

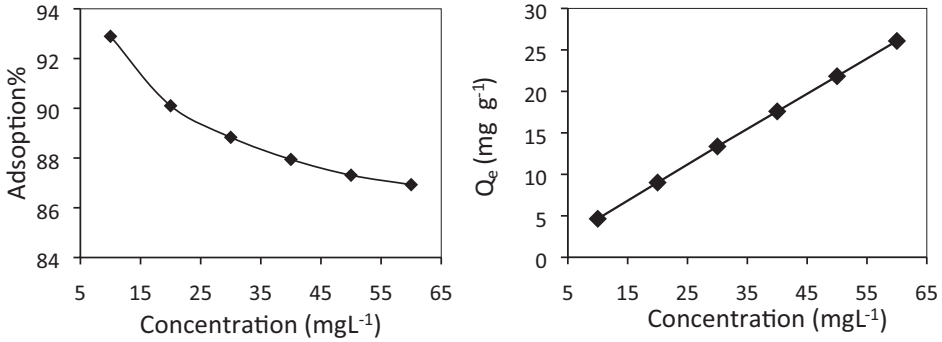

Fig. 9b. Effect of AM concentration on uptake capacity of functionalized-CuO NPs.

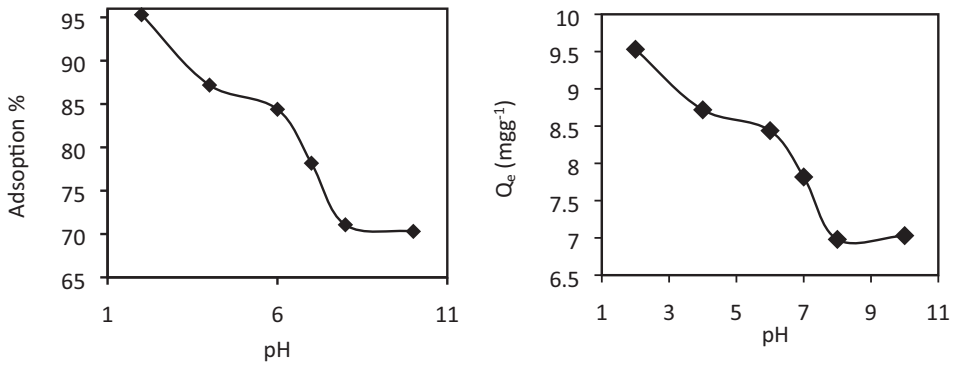

Fig. 9c. Effect of pH on AM uptake percentage of functionalized-CuO NPs.

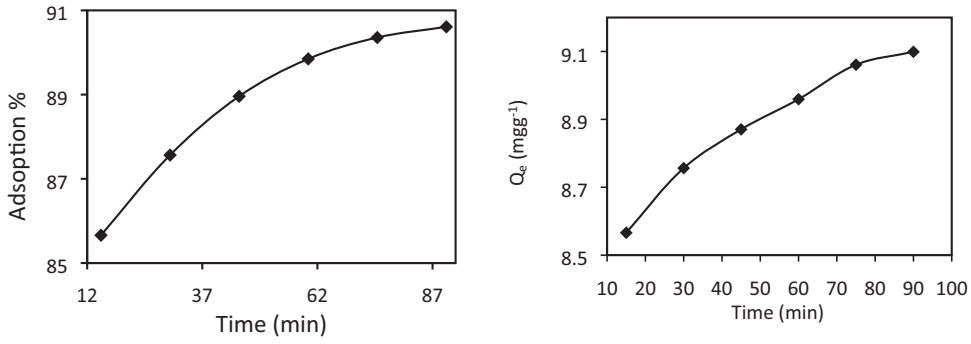

Fig. 9d. Effect of time on the adsorption capacity of functionalized-CuO NPs.

line pH, deprotonation of surface may occur, which leads to the negative charge generation on the surface of solid. Therefore, at alkaline pH, the positively charged adsorbate ions gets easily attached to the negatively charged surface and negatively charged adsorbate ions are repelled by negatively charged surface. Similar to this, the protonation of surface occurs at acidic pH which leads to the positive charge on the surface. Therefore, the effect of variation of surface charge of an adsorbent on the change in the pH can easily be understood from the zero point charge, ZPC, of an adsorbent. At pH above the ZPC, deprotonation of surface occur groups and at pH below the ZPC protonation of groups at the surface occur which leads to the change in the overall charge of adsorbent surface and interaction behaviour.

For this study, the variation of sorption of anionic AM dye onto functionalized-CuO surface with change in pH indicated that once pH was increased the adsorption of AM dye decreased which might be due to repulsion between negatively charged AM from the negatively charged deprotonated surface of CuO. When pH was lowered from 7.7 (ZPC = 7.7 where surface is neutral) to 2.0 the adsorption of AM dye got increased due to the protonation of functionalized-CuO surface. The CuO exists as Cu~OH and at pH below the ZPC of CuO, the surface of CuO became overall positive ($Cu\sim OH_2^+$) and attraction of anionic AM dye and $Cu\sim OH_2^+$ increased (Fig. 9c). When the pH was raised beyond the pH 7.7 the adsorption capacity of functionalized-CuO NPs decreased which might be due to the deprotonation of functionalized-CuO (CuO~OH) surface, and thus surface of CuO became partially negative ($Cu\sim O^-$) which decreased attractive forces for anionic AM dye ions towards the adsorption sites. Therefore, acidic pH of the environment was suitable for better adsorption of AM dye onto the functionalized-CuO NPs surface.

3.3.4. Effect of contact time

Contact time for the reaction between adsorbate and adsorbent largely affects the adsorption capacity and is a major parameter to evaluate the speed of the process. The variation in adsorption percentage (of 2.0 g L^{-1} of CuO for 20 mg L^{-1} concentration of AM dye) with the change in contact time is shown in Fig. 9d. The sorption of AM dye increased gradually with the increase in contact time, and attained maximum at 60 min a after which equilibrium was established between AM dye molecules in the solution and on the surface of adsorbent, thus no net increase in adsorption was noticed. The reason behind this behaviour was that initially all the adsorptive sites on functionalized-CuO NPs were vacant and got readily occupied by AM dye molecules. That is why more than 85% of dye got adsorbed onto CuO surface within 15 min. When contact time was increased the chances of collision also increased which resulted increase in adsorption capacity. However, after certain period of time all the vacant sites on the CuO surface get occupied thus no more adsorption occurred and then reaction attained equilibrium.

3.3.5. Kinetic study

The adsorption data was applied to different kinetic models for understanding the kinetic behaviour of the adsorption of AM dye onto functionalized-CuO NPs. The kinetics of the adsorption generally depends on the intrinsic behaviour of the material as well as nature of pollutants, and also on the experimental conditions. In adsorption process, adsorbate molecules move to solid surface from solution through different steps which control the whole process. This phenomenon can be understood by the fitting adsorption data to different kinetic relationships. For this study, nonlinear forms of pseudo-first order [Fig. S3; Supplementary Information], and pseudo-second order (Fig. 10) were used to determine the kinetic parameters [38–40]. The best fit was obtained by comparing the correlation coefficients (R^2) and the reduced chi square, χ^2, as shown in Table 1. The non-linear forms of pseudo-first and second orders equation are:

$$\frac{dQ_t}{dt} = k_1\left(Q_e - Q_t\right) \tag{4}$$

$$\frac{dQ_t}{dt} = k_2(Q_e - Q_t)^2 \tag{5}$$

where both Q_e and Q_t, in mg g^{-1}, represent the adsorption capacity at equilibrium state and at any time t, respectively. k_1 (min^{-1}), and k_2 (g mg^{-1} min^{-1}) are pseudo-first, and pseudo-second order rate constants, respectively. The results of these rate relationships are summarised in Table 1.

It was concluded from the R^2 values of nonlinear plots that the adsorption of AM dye onto functionalized-CuO NPs could be more correlated to the pseudo-second order (R^2 = 0.90, at 30°C) than that for pseudo-first order kinetic relationship (R^2 = 0.55, at 30°C) used for fitting of the data. Moreover, the difference between the theoretical removal capacity, calculated from the pseudo-second order plot (9.104 mg g^{-1}), and that obtained from the experiments (8.959 mg g^{-1}) were closer than calculated from the pseudo-first order plot (8.155 mg g^{-1}). Beside R^2, the reduced chi square, χ^2, was found to be lower for pseudo-second order plot which clearly suggested that PSO model best fitted to the applied experimental data for the tested AM dye. The result of fitting of the experimental adsorption data to the pseudo-second order relationship suggested that the sorption might be due to simple chemical interaction between

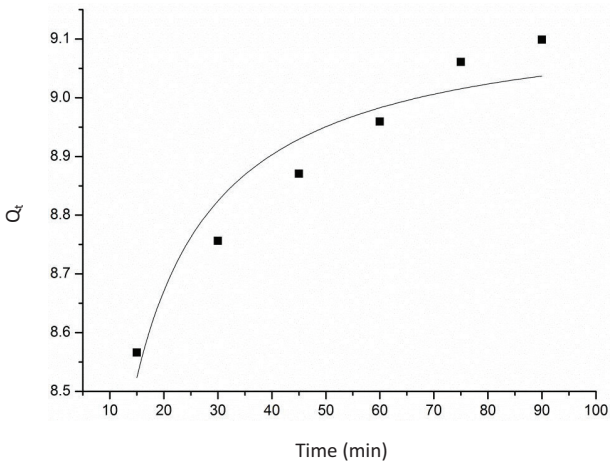

Fig. 10. Nonlinear pseudo-second order kinetic plot.

Table 1
Nonlinear kinetics parameter for adsorption of AM onto functionalized-CuO NPs

Pseudo-first order Q_e(Exp) = 8.96 mg g^{-1}				Second order Q_e(Exp) = 8.96 mg g^{-1}			
k_1 (min^{-1})	Q_e(cal) (mg g^{-1})	R^2	χ^2	k_2 (g mg^{-1} min^{-1})	Q_e(cal) (mg g^{-1})	R^2	χ^2
0.206	8.15	0.55	0.017	0.99	9.14	0.90	0.004

AM ions and the functional groups on the CuO surface. The interaction could be further demonstrated from the FT-IR spectrum of AM loaded CuO surface. However, the interaction between the AM and CuO NPs was weak which could be demonstrated by the desorption study of AM dye loaded CuO NPs. Also, as per pseudo-second order the adsorption rate depends on the concentration of solute molecules and density of adsorptive sites on material. Thus, the adsorption of AM dye on the functionalized-CuO NPs followed the pseudo-second order kinetics.

3.3.6. Temperature effect: Thermodynamics and isotherms

The temperature of the aqueous system affected the adsorption of AM dye from its solution (10–60 mg L^{-1} concentration range, and 2.0 g L^{-1} CuO dosage) which was investigated at 27, 35, and 45ºC. The adsorption of AM dye slightly decreased when the temperature of the solution was raised which suggested the existence of some weak bonds between AM dye and the functionalized-CuO NPs that might have broken down at higher temperature (35 and 45ºC) [Fig. S4; Supplementary Information].

Thermodynamic parameters are evaluated by changing temperature of the reaction mixture to estimate the spontaneity, feasibility, and enthalpy of the overall adsorption process. Change in Gibb's free energy, ΔG°, entropy, ΔS°, and enthalpy, ΔH°, thermodynamic parameters which give information related to the feasibility, spontaneity, and the enthalpy of the adsorption process, were calculated from Van't Hoff equation [41,42] [Fig. S5; Supplementary Information]:

$$\Delta G^o = \Delta H^o - T\Delta S^o \tag{6}$$

$$\Delta G^o = -RT\ln b \tag{7}$$

$$\ln b = \frac{\Delta S^o}{R} - \frac{\Delta H^o}{RT} \tag{8}$$

For the present study, ΔG°, found to be –5.395, –4.256 and –1.256 kJ mol^{-1}, in the range of 0–20 kJ mol^{-1} suggest that the sorption of AM dye onto the functionalized-CuO NPs was spontaneous and proceeded through the physical interaction. Moreover, ΔH°, found to be +0.002 kJ mol^{-1}, suggested that the process was endothermic, and the same was further confirmed from the D-R isotherm. The negative ΔS° (–0.628 kJ K^{-1} mol^{-1}) indicated the potent binding forces operating during the adsorption of AM dye toward CuO NPs [43].

The information about distribution of adsorbate between liquid and solid phases is studied to know mechanisms, surface properties, and affinities of the adsorbate molecules towards adsorbent surface can be estimated from isotherm studies. The nonlinear plots of three isotherms, namely, Langmuir, Freundlich, and Dubinin-Radushkevich, were used to fit the experimental data obtained from this study to get the best fit isotherm.

Langmuir isotherm (Fig. 11a) is a well known model which assumes that one site on the surface of adsorbent is occupied only by one molecule/ion of adsorbate and the adsorption energy is constant. The nonlinear form of Langmuir isotherm is given below [44–46]:

$$Q_e = \frac{Q_o b C_e}{1 + bC_e} \tag{9}$$

where Q_o (mg g^{-1}) is maximum adsorption capacity of an adsorbent, and b (L mg^{-1}) is a Langmuir constant, both can be calculated from the above equation. The value of Q_o, obtained from nonlinear Langmuir plot, decreased from 55.33 to 33.17 mg g^{-1} when the temperature of the reaction mixture was increased from 27 to 45°C, respectively. The maximum adsorption capacity of the functionalized-CuO NPs was noted higher than previously reported adsorbents (Table 4). The values of the Langmuir constant, b, was found in the range 0–1 L mg^{-1} which indicated weak binding of AM dye onto the functionalized-CuO NPs surface at lower temperature and with the rise in temperature it increased (Table 2). The regression coefficients indicated good fitting of the adsorption data at higher temperature and slightly poor at lower temperature [46,47]. The separation factor R_L, another parameter of Langmuir isotherm, is defined as:

$$R_L = \frac{1}{(1 + bC_o)} \tag{10}$$

The R_L value, found in the range $0 < R_L < 1$,revealed that the sorption of AM dye onto functionalized-CuO NPs was energetically favourable at 27–45ºC temperature range.

Freundlich isotherm, based on the concept of non-uniform distribution of heat of adsorption over a heterogeneous surface and multilayer sorption, is given as [1,47]:

$$Q_e = k_F C_e^{\frac{1}{n}} \tag{11}$$

where k_F (mg$^{(1-n)}$ L^{n}g^{-1}) and n are Freundlich constants and represent the capacity of an adsorbent, and the intensity of the adsorption process, respectively. For the nonlinear plot (Fig. 11b), the k_F value was found in range 5.662 to 10.436 mg$^{(1-n)}$ L^n g^{-1}. The values of n, found in the range 1–10, indicated favourable adsorption process having good interactions between AM dye and functionalized-CuO NPs and heterogeneity of the adsorbent surface (Table 2).

The nature of the adsorption process can also be evaluated by the fitting of experimental adsorption data to Dubinin-Radushkevich isotherm (D-R) (Fig. 11c) which also gives the relation between the porous structure and adsorption by the adsorbate. The nonlinear form of this model is [46]:

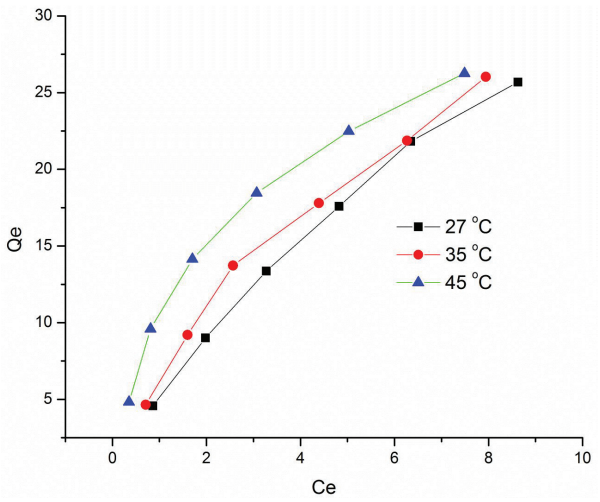

Fig. 11a. Nonlinear Langmuir adsorption isotherm plot for AM adsorption.

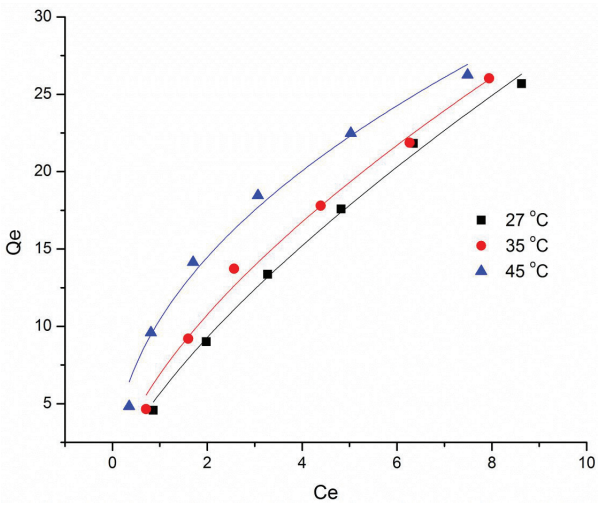

Fig. 11b. Nonlinear Freundlich adsorption isotherm plot for AM adsorption.

$$Q_e = Q_{D-R}\exp(-\beta\varepsilon^2) \tag{12}$$

where $Q_{D\text{-}R}$, and β (mol² kJ⁻²) are theoretical capacity, and mean free energy of adsorption, respectively. Moreover, the β is also related to the equilibrium concentration, ε, called Polyani potential, and can be calculated from the relationship [46]:

$$RT\ln\left(1+\frac{1}{C_e}\right)=\varepsilon \tag{13}$$

As given in the Table 2, the calculated $Q_{D\text{-}R}$ value was found in the range 25.479 to 23.312 mg g^{-1}. The constant β is also related to the mean free energy of adsorption, E (kJ mol^{-1}), asgiven below [46]:

$$E_{D-R}=(-2\beta)^{-0.5} \tag{14}$$

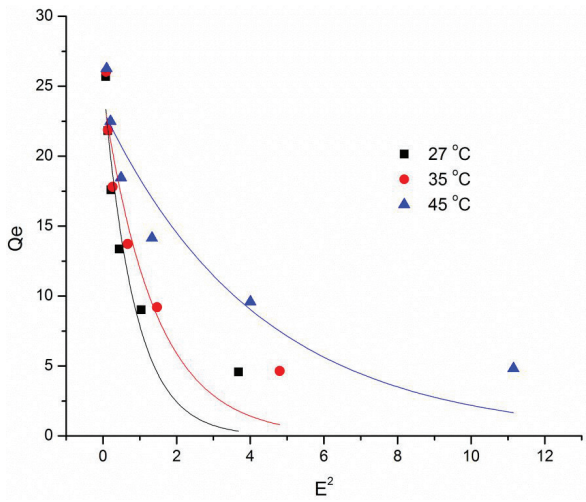

Fig. 11c. Nonlinear Dubinin-Radushkevich isotherm plot for AM adsorption.

For the present study, the values of $E_{D\text{-}R}$ was found to be less than 8.0 kJ mol^{-1} (in the range 0.652–1.453) in the temperature range 27–45°C, which suggested that the adsorption of AM dye onto functionalized-CuO NPs was a physical process [39]. From these nonlinear plots, the higher R^2 value and lower χ^2_{error} of Freundlich isotherm confirmed that the AM dye adsorption onto the functionalized-CuO NPs surface followed the Freundlich isotherm which revealed the heterogeneity of adsorbent surface.

3.3.7. Mechanism

The present adsorption process, as discussed above, was a physical process; therefore, the transfer of AM dye molecules from aqueous medium to the solid surface can be understood by intraparticle diffusion, and film diffusion action. The experimental kinetics data was applied to both the models and result are given in Table 3.

In brief, intra-particle diffusion model (IPD), based on the chemical interaction between the adsorbate and interior pores on the solid surface, is slowest step then according to Weber and Morris, the solute uptake varies proportionally with $t^{0.5}$ and the following relationship will be applicable to the system [46] (Fig. 12):

$$Q_t = k_{ipd}t^{0.5} + C \tag{15}$$

where k_{ipd} is rate constant for intraparticle diffusion process and equal to the slope of plot. The k_{ipd} was found to be 0.096 mg g^{-1} min$^{0.5}$, with 8.215 intercept of the straight line having nearly unit regression coefficient. Furthermore, if the adsorbate molecules have to pass the liquid film around the solid surface to get adsorbed then the liquid film diffusion model (LFD) is applied as [46] [Fig. S6; Supplementary Information]:

$$\ln(1-F) = -k_{fd}t \tag{16}$$

where $F = Q_t/Q_e$, and k_{fd} is the rate constant for diffusion of liquid film by the adsorbate whose value was found, as

Table 2
The nonlinear isothermal parameters for the adsorption of AM onto functionalized-CuO NPs

Temp. (°C)	Langmuir					Freundlich				Dubinin-Radushkevich				
	Q_o (mg g^{-1})	b (L mg^{-1})	R_L	R^2	χ^2	k_F (mg$^{(1-n)}$	n L^{n}g^{-1})	R^2	χ^2	Q_{DR} (mg g^{-1})	β (mol^2 kJ^{-2})	E (kJ mol^{-1})	R^2	χ^2
27	55.33	0.207	0.039	0.91	78.54	5.663	1.403	0.99	0.317	25.479	1.173	0.652	0.86	8.297
35	45.54	0.069	0.012	0.92	79.33	6.902	1.564	0.99	0.572	24.438	0.711	0.838	0.87	8.178
45	33.17	0.446	0.100	0.99	0.485	10.436	2.125	0.98	1.042	23.312	0.236	1.453	0.86	8.956

Table 3
Film and intraparticle diffusion parameters for adsorption of AM onto functionalized-CuO NPs

Film diffusion model			Intraparticle diffusion model		
k_{fd} (mg g^{-1} min^{-1})	Intercept	R^2	k_{ipd} (mg g^{-1} min$^{0.5}$)	Intercept	R^2
0.329	4.633	0.68	0.096	8.215	0.99

Table 4
The comparative Amaranth adsorption study of functionalized-CuO NPs to other adsorbents

Adsorbent name	Amaranth removal capacity (mg g^{-1})	Ref.
Fe_3O_4/MgO	37.98	[48]
Iron oxide nanoparticles (IONPs) coated with cetyltrimethylammonium bromide (CTAB)	1.05	[49]
Alumina reinforced polystyrene composites	20.2	[50]
Bottom ash	7.80	[51]
E. Crassipes leaves	43.1	[52]
E. Crassipes roots	28.51	
E. Crassipes stems	23.97	
Potato peels	1.709	[53]
Guava leaves	1.028	
Functionalized-CuO NPs	55.33	This Study

slope, from the straight line plot between *ln(1–F)* and time *t* that passes through the origin. The film diffusion rate constant, k_{fd}, calculated to be 0.329 mg g^{-1}min^{-1} with intercept of 4.633 and 0.68 regression coefficient [Fig. S6; Supplementary Information]. However, the regression coefficient value suggested the poor fitting of kinetic data to the LFD relationship. Therefore, intraparticle diffusion might be controlling the rate of AM dye adsorption on to the CuO surface.

3.3.8. Removal of CR and BBR by functionalized-CuO NPs

Functionalized-CuO NPs were also used for the adsorption of two other toxic dyes, Congo red (CR), and Bismarck brown R (BBR). The obtained results showed that about 80% of CR and 47% of BBR could be adsorbed from the aqueous

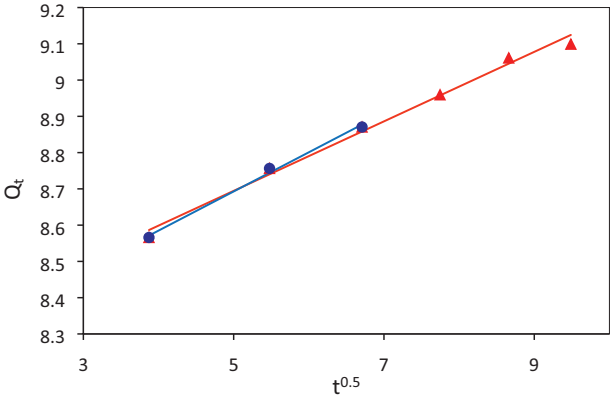

Fig. 12. Intraparticle diffusion plot for AM adsorption.

media having concentration of 10 mg L^{-1}, respectively, with 2.0 g L^{-1} of functionalized-CuO NPs. Thus, the functionalized-CuO NPs is also efficient material for adsorption of CR and BBR. Although the capacity was inferior for CR and BBR than that for AM dye, therefore, biogenic functionalized-CuO NPs can be efficiently employed for treatment of water containing various types of organic dyes.

3.3.9. Reusability of exhausted functionalized CuO NPs

The regeneration of exhausted functionalized-CuO NPs was achieved by tuning pH of the solution using 0.1 M NaOH and then the reusability was checked by running the number of adsorption-desorption cycles. It was found that no significant reduction in the adsorption capacity of the functionalized-CuO NPs was noticed after three adsorption-desorption cycle.

4. Conclusion

The water pollution due to dyes, released through industrial wastewater, is associated with skin irritation, allergic, mutagenic, carcinogenic and others severe diseases. So, their removal from water is essential and the adsorption is promising method for that. CuO NPs has got so much attention as smart and advance material for the removal of many hazardous azo dyes that cause water pollution.

But the conventional method creates more water pollution, therefore, an eco-friendly green method was preparation and also for enhancing the capacity, these particles were functionalized using Brassica rapa leaves, an easily

available and possessing many active phytochemicals. The functionalized-CuO NPs showed high adsorbing capacity, in batch mode experiments, for Amaranth dye, studied in terms concentration, dosage, pH, temperature. CuO NPs showing the Langmuir adsorption capacity of 55.33 mg $g^{-1}$and data fitted better to Freundlich isotherm, and kinetics followed pseudo-second order relationship indicating specific site interaction. Thus, functionalized-CuO NPs proved to be a cost-effective and high adsorption capacity material for reducing the water contamination caused by dyes.

Acknowledgement

Authors gratefully acknowledged the support provided by the Jamia Millia Islamia, New Delhi, India, for carrying out the present research work.

References

[1] S.I. Siddiqui, S.A. Chaudhry, Nigella sativa plant based nanocomposite-$MnFe_2O_4$/BC: A non-toxic, antibacterial material for water purification application, J. Clean. Prod., 200 (2018) 996–1008.
[2] Y. Yao, L. Wang, L. Sun, S. Zhu, Z. Huang, Y. Mao, W. Lu, W. Chen, Efficient removal of dyes using heterogeneous fenton catalysts based on activated carbon fibres with enhanced activity, Chem. Eng. Sci., 101 (2013)424–431.
[3] S.I. Siddiqui, R. Ravi, G. Rathi et al., Decolorization of textile wastewater using composite materials, In Nanomaterials in the wet processing of textiles, Ed., S.U. Islam, B.S. Butola, John Wiley & Sons, Inc., 2018, pp. 187–218. https://doi.org/10.1002/9781119459804.
[4] S.I. Siddiqui, B. Fatima, N. Tara, G. Rathi, S.A. Chaudhry, 15: Recent advances in remediation of synthetic dyes from wastewaters using sustainable and low-cost adsorbents, In The textile institute book series, The impact and prospects of green chemistry for textile technology, Ed., S.U. Islam, B.S. Butola, Woodhead Publishing, Elsevier, 2019, pp. 471–507. https://doi.org/10.1016/B978-0-08-102491-1.00015-0.
[5] D. Rawat, V. Mishra, R.S. Sharma, Detoxification of azo dyes in the context of environmental processes, Chemosphere, 155 (2016) 591–605.
[6] M. Tokumura, H.T. Znad, Y. Kawase, Modelling of an external light irradiation slurry photoreactor: UV light or sunlight-photo assisted Fenton discoloration of azo-dye Orange II with natural mineral tourmaline powder, Chem. Eng. Sci., 61 (2006) 6361–6371.
[7] N. Divya, A. Bansal, A.K. Jana, Photocatalytic activity of transition metal ion doped Titania for Amaranth dye degradation, Mater. Sci. Forum., 712 (2012) 85–104.
[8] E.M. Elgendy, N.A. Al-Zahrani, Comparative study of natural and synthetic food additive dye amaranth through photochemical reactions, Indian J. Sci. Res., 4 (2015) 827–832.
[9] H. Sudrajat, S. Babel, H. Sakai, S. Takizawa, Rapid photocatalytic degradation of the recalcitrant dye amaranth by highly active N-WO3, Environ. Chem. Lett., 165 (2015) 224–234.
[10] S.I. Siddiqui, M. Naushad, S.A. Chaudhry, Promising prospects of nanomaterials for arsenic water remediation: A comprehensive review, Process Saf. Environ. Protect., 126 (2019) 60–97.
[11] S.I. Siddiqui, S.A. Chaudhry, Nanohybrid composite Fe_2O_3-ZrO_2/BC for inhibiting the growth of bacteria and adsorptive removal of arsenic and dyes from water, J. Clean. Prod., 223 (2019) 849–868.
[12] L. Fu, G. Zhang, S. Wang, L. Zhang, J. Peng, Modification of activated carbon via grafting polyethyleneimine to remove amaranth from water, Appl. Water Sci., 7 (2017) 4247–4254.
[13] S.I. Siddiqui, S.A. Chaudhry, A review on graphene oxide and its composite preparation and its use for the removal of $As^{3+}$and As^{5+} from water under various parameters: Application of isotherm, kinetic and thermodynamics, Process Saf. Environ. Protect., 119 (2018) 138–163.
[14] S.I. Siddiqui, G. Rathi. S.A. Chaudhry, Qualitative analysis of acid washed black cumin seeds for decolourization of water through removal of highly intense dye methylene blue, Data in Brief, 20 (2018) 1044–1047.
[15] N. Tara, S.I. Siddiqui, G. Rathi, S.A. Chaudhry, Inamuddin, A.M. Asiri, Nano-engineered adsorbent for the removal of dyes from water: A review, Curr. Anal. Chem., 15(1) (2019).
[16] S.I. Siddiqui, S.A. Chaudhry, Arsenic removal from water using nanocomposites: a review, Curr. Environ. Eng., 4 (2017) 81–102.
[17] S.I. Siddiqui, S.A. Chaudhry, Arsenic: toxic effects and remediation. In Advanced materials for wastewater treatment, Ed., S.U. Islam, John Wiley & Sons, Inc., 2017, pp. 1–27. https://doi.org/10.1002/9781119407805.ch1.
[18] S.I. Siddiqui, S.A. Chaudhry, Iron oxide and its modified forms as an adsorbent for arsenic removal: a comprehensive recent advancement, Process Saf. Environ. Protect., 111 (2017) 592–626.
[19] S.I. Siddiqui, S.A. Chaudhry, Removal of arsenic from water through adsorption onto metal oxide-coated material, Mater. Res. Found., 15 (2017) 227–276.
[20] K.J. McDonald, B. Reynolds, K.J. Reddy, Intrinsic properties of cupric oxide nanoparticles enable effective filtration of arsenic from water, Sci. Rep., 5 (2015) 11110.
[21] S.A. Chaudhry, T.A. Khan, I. Ali, Adsorptive removal of Pb(II) and Zn(II) from water onto manganese oxide-coated sand: Isotherm, thermodynamic and kinetic studies, Egypt. J. Basic Appl. Sci., 3 (2016) 287–300.
[22] H.R. Naika, K. Lingaraju, K. Manjunath, D. Kumar, G. Nagaraju, D. Suresh, H. Nagabhushana, Green synthesis of CuO nanoparticles using Gloriosa superba leaf extract and their antibacterial activity, J. Taibah Univ. Sci., 9 (2015) 7–12.
[23] P.P.N.V. Kumar, U. Shameem, P. Kollu, R.L. Kalyani, S.V.N. Pammi, Green synthesis of copper oxide nanoparticles using aloe vera leaf extract and its antibacterial activity against fish bacterial pathogens, J. Bionanosci., 5 (2015) 135–139.
[24] S.M. Yedurkar, C.B. Maurya, P.A. Mahanwar, A biological approach for the synthesis of copper oxide nanoparticles by the ixora coccinea leaf extract, J. Mater. Environ. Sci., 8 (2017) 1173–1178.
[25] G.M. Sulaiman, A.T. Tawfeeq, M.D. Jaaffer, Biogenic synthesis of copper oxide nanoparticles using oleaeuropea leaf extract and evaluation of their toxicity: An in vivo and in vitro study, Biotechnol. Prog., 34 (2018) 218–230.
[26] P. Sutradhar, M. Saha, D. Maiti, Microwave synthesis of copper oxide nanoparticles using tea leaf and coffee powder extracts and its antibacterial activity, J. Nanostruct Chem., 4 (2014) 86.
[27] A. Thit, K. Huggins, H. Selck, A. Baun, Acute toxicity of copper oxide nanoparticles to Daphnia magna under different test conditions, Toxicol. Envirom. Chem., 99 (2016) 1–15.
[28] M.E. Cartea, M. Francisco, P. Soengas, P. Velasco, Phenolic compounds in Brassica vegetables, Molecules, 16 (2011) 251–280.
[29] M.I. Din, F. Arshad, A. Rani, et al., Single step green synthesis of stable F-CuO NPs as efficient photo catalyst material, J. Opt. Electron. Biomed. Mater., 9 (2017) 41–48.
[30] H. Hosseinzadeh, S. Mohammadi, Quince seed mucilage magnetic nanocomposites as novel bioadsorbents for efficient removal of cationic dyes from aqueous solutions, Carbohydr. Polym., 134 (2015) 213–221.
[31] T.A. Khan, S.A. Chaudhry, I. Ali, Equilibrium uptake, isotherm and kinetic studies of Cd (II) adsorption onto iron oxide activated red mud from aqueous solution, J. Mol. Liq., 202 (2015) 165–175.
[32] V.V.T. Padil, M. Cernik, Green synthesis of F-CuO NPs using gum karaya as a biotemplate and their antibacterial application, Intern. J. Nanomed., 8 (2013) 889–898.

[33] K. Abdellaoui, I. Pavlovic, M. Bouhent, Mustapha, A. Benhamou, C. Barriga, A comparative study of the amaranth azo dye adsorption/desorption from aqueous solutions by layered double hydroxides. Appl. Clay Sci., 143 (2017) 142–150.
[34] A. Momin, R. Pervin, J. Uddin, G.M. Khan, M. Islam, One step synthesis and optical evaluation of CuO NPs, J. Bangladesh Electron. Soc., 10 (2010) 57–63.
[35] J. Ramyadevi, K. Jeyasubramanian, A. Marikani, G. Rajakumar, Copper nanoparticles synthesized by polyol process used to control hematophagous parasites, Parasitology Res., 109 (2011) 1403–1415.
[36] T.A. Khan, S.A. Chaudhry, I. Ali, Thermodynamic and kinetic studies of As (V) removal from water by zirconium oxide–coated marine sand, Environ. Sci. Pollut. Res., 20 (2003) 5425–5440.
[37] F. Marabelli, G.B. Parravicini, F. Salghetti-Drioli, Optical gap of Cu, Phys. Rev. B., 52 (1995) 1433.
[38] S.A. Chaudhry, T.A. Khan, I. Ali, Equilibrium, kinetic and thermodynamic studies of Cr (VI) adsorption from aqueous solution onto manganese oxide coated sand grain (MOCSG), J. Mol. Liq., 236 (2017a) 320–330.
[39] S.A. Chaudhry, T.A. Khan, I. Ali, Zirconium oxide-coated sand-based batch and column adsorptive removal of arsenic from water: Isotherm, kinetic and thermodynamic studies, Egypt. J. Petrol., 26 (2017b) 553–563.
[40] S.A. Chaudhry, Z. Zaidi, S.I. Siddiqui, Isotherm, kinetic and thermodynamics of arsenic adsorption onto iron-zirconium binary oxide-coated sand (IZOBCS): modelling and process optimization, J. Mol. Liq., 229 (2017c) 230–240.
[41] S.A. Chaudhry, M. Ahmed, S.I. Siddiqui, S. Ahmed, Fe (III)–Sn (IV) mixed binary oxide-coated sand preparation and its use for the removal of As(III) and As(V) from water: application of isotherm, kinetic and thermodynamics, J. Mol. Liq., 224 (2016) 431–441.
[42] S.A. Chaudhry, T.A. Khan, I. Ali, Adsorptive removal of Pb (II) and Zn (II) from water onto manganese oxide-coated sand: Isotherm, thermodynamic and kinetic studies, Egypt. J. Basic Appl. Sci., 3 (2016) 287–300.
[43] Z. Aghili, S. Taheri, H.A. Zeinabad, L. Pishkar, A.A. Saboury, A. Rahimi, M. Falahati, Investigating the interaction of Fe nanoparticles with lysozyme by biophysical and molecular docking studies, Plos One., 11 (2016) 0164878.
[44] S.I. Siddiqui, O. Manzoor, M. Mohsin, S.A. Chaudhry, Nigella sativa seed based nanocomposite-MnO_2/BC: An antibacterial material for photocatalytic degradation, and adsorptive removal of dye from water, Environ. Res., 171 (2019) 328–340.
[45] X. Wang, C. Jiang, B. Hou, Y. Wang, C. Hao, J. Wu, Carbon composite lignin-based adsorbents for the adsorption of dyes, Chemosphere, 206 (2018) 587–596.
[46] S.I. Siddiqui, G. Rathi, S.A. Chaudhry, Acid washed black cumin seed powder preparation for adsorption of methylene blue dye from aqueous solution: Thermodynamic, kinetic and isotherm studies, J. Mol. Liq., 264 (2018) 275–284.
[47] Y. Wang, L. Zhu, X. Wang et al., Synthesis of aminated calcium lignosulfonate and its adsorption properties for azo dyes, J. Indus. Eng. Chem., 61 (2018) 321–330.
[48] A. Naby, M. Salem, M.A. Ahmed, M.F. El-Shahat, Selective adsorption of amaranth dye on Fe_3O_4/MgO nanoparticles, J. Mol. Liq., 219 (2016) 780–788.
[49] B. Zargar, H. Parham, A. Hatamie, Fast removal and recovery of amaranth by modified iron oxide magnetic nanoparticles, Chemosphere, 76 (2009) 554–557.
[50] R. Ahmad, R. Kumar, Adsorption of amaranth dye onto alumina reinforced polystyrene, Clean Soil Air Water, 39 (2011) 74–82.
[51] A. Mittal, L.K. Krishnan, V.K. Gupta, Use of waste materials – bottom ash and de-oiled soya, as potential adsorbents for the removal of amaranth from aqueous solutions, J. Hazard. Mater., 117 (2005) 171–178.
[52] I.G. Coronilla, L.M. Barrera, T.L.V. Garrido, E.C. Urbina, Biosorption of amaranth dye from aqueous solution by roots, leaves, stems and the whole plant of E. Crassipes, Environ. Eng. Manage. J., 13 (2014) 1917–1926.
[53] R. Rehman, T. Mahmud, M. Irum, Comparative sorption studies for amaranth dye removal from water in cost-effective way using guava leaves and potato peels, Asian J. Chem., 27 (2015) 2008–2014.

Supplementary

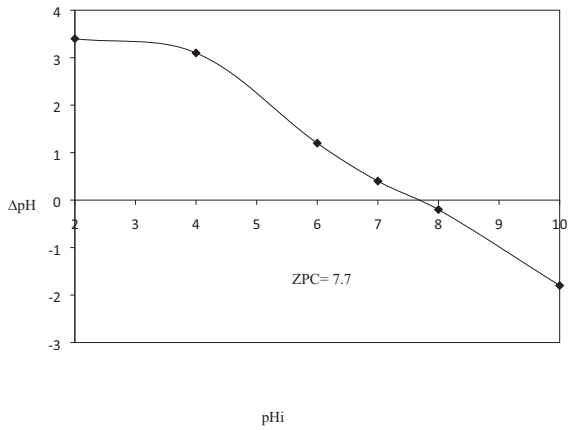

Fig. S1. Zero point charge of functionalized-CuO NPs.

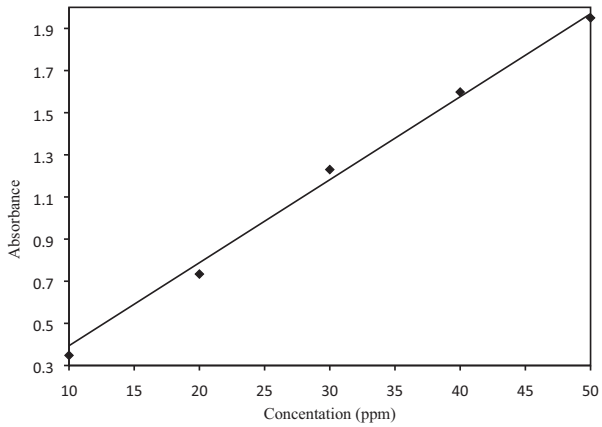

Fig. S2. Calibration curve for AM.

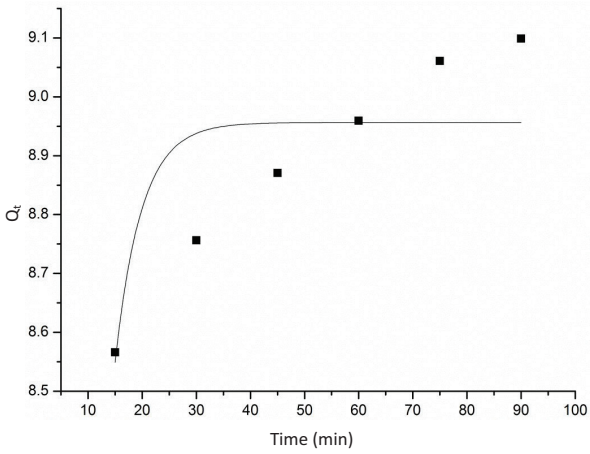

Fig. S3. Nonlinear plot of pseudo first order kinetics for AM adsorption.

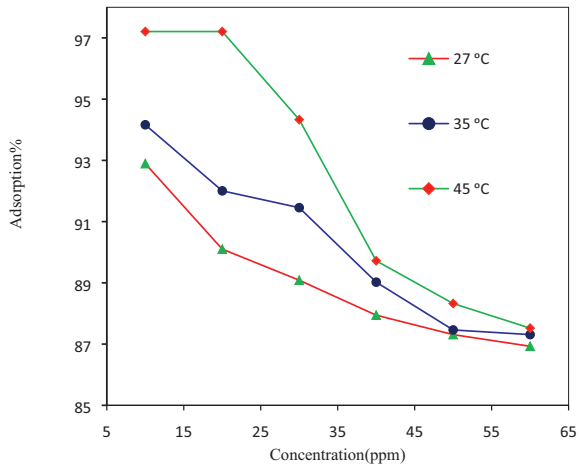

Fig. S4. Effect of temperature on AM adsorption onto functionalized-CuO NPs surface.

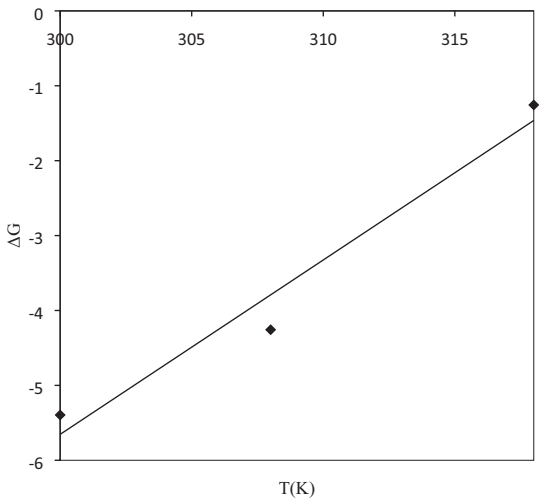

Fig. S5. Thermodynamics plots, ΔG Vs T(K) of AM adsorption.

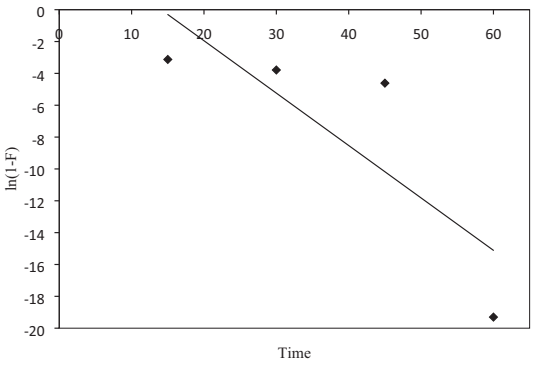

Fig. S6. Film diffusion plot for AM adsorption